JBC RESEARCH ARTICLE

SUMOylation of microtubule-cleaving enzyme KATNA1 promotes microtubule severing and neurite outgrowth

Received for publication, June 15, 2022, and in revised form, July 10, 2022 Published, Papers in Press, July 20, 2022,
https://doi.org/10.1016/j.jbc.2022.102292

Shaojin Li[‡], Yaozhong Liang[‡], Jianyu Zou, Zhenbin Cai, Hua Yang, Jie Yang, Yunlong Zhang, Hongsheng Lin[*], Guowei Zhang[*], and Minghui Tan[*]

From the Department of Orthopaedics, The First Affiliated Hospital of Jinan University, Guangzhou, China

Edited by George DeMartino

Katanin p60 ATPase-containing subunit A1 (KATNA1) is a microtubule-cleaving enzyme that regulates the development of neural protrusions through cytoskeletal rearrangements. However, the mechanism underlying the linkage of the small ubiquitin-like modifier (SUMO) protein to KATNA1 and how this modification regulates the development of neural protrusions is unclear. Here we discovered, using mass spectrometry analysis, that SUMO-conjugating enzyme UBC9, an enzyme necessary for the SUMOylation process, was present in the KATNA1 interactome. Moreover, GST-pull down and co-immunoprecipitation assays confirmed that KATNA1 and SUMO interact. We further demonstrated using immunofluorescence experiments that KATNA1 and the SUMO2 isoform colocalized in hippocampal neurites. We also performed a bioinformatics analysis of KATNA1 protein sequences to identify three potentially conserved SUMOylation sites (K77, K157, and K330) among vertebrates. Mutation of K330, but not K77 or K157, abolished KATNA1-induced microtubule severing and decreased the level of binding observed for KATNA1 and SUMO2. Cotransfection of SUMO2 and wildtype KATNA1 in COS7 cells increased microtubule severing, whereas no effect was observed after cotransfection with the K330R KATNA1 mutant. Furthermore, in cultured hippocampal neurons, overexpression of wildtype KATNA1 significantly promoted neurite outgrowth, whereas the K330R mutant eliminated this effect. Taken together, our results demonstrate that the K330 site in KATNA1 is modified by SUMOylation and SUMOylation of KATNA1 promotes microtubule dynamics and hippocampal neurite outgrowth.

Katanin is a microtubule-cleaving enzyme that is a member of the AAA+ protein family (1). Katanin is a heterodimer composed of two subunits, including the catalytic subunit KATNA1 (Katanin p60 ATPase-containing subunit A1), which contains the AAA+ ATPase domain, and the regulatory subunit p80 (2). Microcephaly is a neurodevelopmental disorder, wherein mutations in Katanin cause increased centrosome numbers and spindle multipolarity in patients (3). KATNA1 hydrolyzes ATP to release energy to sever microtubules (4). Glycosylation, glutamylation, and acetylation of microtubules enhances the severing efficiency of Katanin, whereas deacetylation effectively terminates Katanin-mediated microtubule severing (5–7). Microtubules are extremely important for neurite outgrowth because they are not only "wagons" for intracellular transport of substances (8, 9) but are also essential for axon and dendrite formation (10). The KATNA1 subunit provides the majority of observed Katanin activity because it includes domains for microtubule interaction, p80 binding, and C large subunit interaction and the AAA+ structural domain (11). KATNA1, abundantly expressed in neuronal cells, plays a critical role in neuronal development by regulating microtubule dynamics (12). Knockdown of KATNA1 inhibits the growth of neuronal axons (13). The expression of KATNA1 is also tightly regulated and is similar to that of Spastin (14). Our previous studies suggest that KATNA1 promotes the growth of neuronal protrusions (15), but the underlying detailed mechanism is unclear.

SUMOylation is a posttranslational modification wherein SUMO is covalently attached to the substrate through a process that is similar to ubiquitination (16). The SUMOylation process requires a series of coenzymes, including activating enzyme E1, binding enzyme E2, and ligase E3, to attach SUMO molecules to target proteins (17). SUMO proteins are highly conserved from yeast to mammals (18). In mammals, there are four isoforms of SUMO: SUMO1, SUMO2, SUMO3 and SUMO4 (16). SUMOylation affects protein stability, protein biochemical activity, protein–protein interactions, and transport processes into the nucleus, thereby playing an important role in regulating cellular biological functions (19, 20). Disruption of SUMOylation leads to a variety of neurological disorders, including neurodegenerative diseases (21), spinal cerebellar ataxia (22), and cerebral ischemia and epilepsy (23). SUMOylation can also affect synaptic plasticity and neurotransmitter transmission (24). Therefore, SUMOylation is predicted to be a therapeutic target for many diseases (25). However, KATNA1 SUMOylation and its respective function in modulating neuronal processes have not been investigated.

To explore the posttranscriptional modification regulatory mechanism of KATNA1 in modulating microtubule severing and neurite outgrowth in neurons, this study tried to determine whether KATNA1 could be SUMOylated and to

[‡] These authors contributed equally to this work.
[*] For correspondence: Minghui Tan, tanminghui@jnu.edu.cn; Hongsheng Lin, tlinhsh@jnu.edu.cn; Guowei Zhang, zgw24@qq.com.

elucidate the detailed molecular mechanism of KATNA1 SUMOylation and the effect of this SUMOylation modification on regulating neuronal development.

Results

KATNA1 interacts with SUMOylating proteins

KATNA1 is modified by ubiquitination (26) and phosphorylation (27). To further explore the posttranslational modification of KATNA1, we used mass spectrometry analysis of the KATNA1 interactome. Brain lysates were pulled down by GST-KATNA1, comparing with GST. The sediments were first determined by silver staining, showing large amount of pulldown sediments in the GST-KATNA1 group (Fig. 1*A*). Then the lanes were subjected to mass spectrometry analysis. Among the variety of interacting proteins with KATNA1, UBC9, which is an E2 SUMO-conjugating enzyme, attracted our attention (Fig. 1*B*). These data suggest that KATNA1 may be SUMOylated. To verify this, we purified GST, GST-SUMO1, GST-SUMO2, GST-SUMO3, and GST-KATNA1 (Fig. 1, *C* and *D*, lower panel) for GST pulldown assays using brain lysates. The Western blotting results from the GST-SUMO pulldowns showed that KATNA1 was present in the sediments for SUMO1 and SUMO2, with SUMO2 having the highest signal (Fig. 1*C*, upper panel). Furthermore, SUMO2 was detected in the sediments for GST-KATNA1 (Fig. 1*D*, upper panel). Next, we overexpressed Flag-UBC9, GFP-KATNA1, and HA-SUMO2 in 293T cells and performed immunoprecipitation (IP) with a HA antibody. As shown in Figure 1*E*, the results revealed that GFP-KATNA1 is detected in the IP sediments, showing the potential SUMOylated KATNA1. Furthermore, rat brain lysates were used to perform IP with the KATNA1 antibody; the results also showed that SUMO2 is present in the sediments (Fig. 1*F*). Cultured hippocampal neurons were immunostained with SUMO2 and KATNA1, and confocal analysis indicated that the two colocalized in the growth protrusions (Fig. 1, *G* and *H*). These data suggest that KATNA1 interacts with SUMO2 and KATNA1 could be SUMOylated.

Acetylation of microtubules promotes KATNA1-mediated severing

KATNA1 is a microtubule severing protein (4). To determine the effect of SUMOylation on KATNA1 function, we chose COS7 cells for microtubule severing assay, because these cells have a flat microtubule skeleton and are convenient for imaging. Simply overexpression of KATNA1 could not induce microtubule severing, and acetylation of microtubules facilitate Katanin to access microtubules for severing in fibroblasts (5). To confirm this, we initially revealed the acetylation level of microtubules in COS7; the results showed that the endogenous microtubules in COS7 were not acetylated (Fig. 2*A*, DMSO group). Therefore, we treated the cells with tubacin, a compound that increases the acetylation of microtubules. This treatment significantly increased the acetylation levels of the microtubules, as evidenced by immunofluorescence staining (Fig. 2, *A* and *B*). The same trend was observed by Western blotting (Fig. 2, *C* and *D*). Pretreatment of the cells with tubacin significantly increased KATNA1-mediated microtubule severing in transfected cells (circled with white line; Fig. 2, *E* and *F*). Thus, COS7 cells were all treated with tubacin for the following experiments to observe the microtubule severing by KATNA1. These data show that acetylation enhances the microtubule severing activity of KATNA1, which is consistent with a previous report (5).

K330 is the SUMOylation site in KATNA1

Next, we determined the detailed molecular bias and the impact of SUMOylation on KATNA1 function. We used bioinformatics analysis to predict the potential SUMOylation sites on KATNA1. The software tools GPS-SUMO 1.0 (28), SUMOsp (29), and PCI-SUMO (30, 31) revealed the presence of three sites in the KATNA1 protein sequence, FKLD (K77), EKKE (K157), and VKAE (K330), which are consistent with the consensus SUMOylation motif (ΨKxE/D, where Ψ is a large hydrophobic amino acid and x is an arbitrary amino acid) (32). These three motifs are conserved among a variety of vertebral species (Fig. 3*A*). To determine the function of each site, we mutated the potential SUMOylation site lysine (K) to arginine (R) in order to eliminate SUMOylation with the smallest impact on protein sequence and property. We constructed KATNA1 single point mutants (K77R, K157R, and K330R) and a triple point mutant (Pan) and overexpressed these plasmids in COS7 cells to observe their microtubule severing ability. Immunofluorescence staining analysis showed that wildtype (WT) KATNA1 (GFP-KATNA1) significantly induced microtubule severing in transfected cells (circled with white line), with the largely decreased fluorescence signals of microtubules (Fig. 3*B*, WT *versus* Control). Pan mutation of the three potential sites abolished the severing activity of KATNA1, revealed by the rescued microtubule fluorescence signals (Fig. 3*B*, Pan *versus* WT). The K330R mutation showed the reduced activity toward microtubule severing as Pan mutation; however, the activities of K77R and K157R mutants were not changed, acting like WT KATNA1 (Fig. 3*B*). The relative fluorescence intensity of microtubules was quantified and shown in Figure 3*C*. These data indicate that K330 SUMOylation is required for the microtubule severing activity for KATNA1, mutation of this site to arginine would abolish the activity of KATNA1. To confirm this, we performed IP assays. Wildtype or K330-mutated KATNA1 (KATNA1 K330R) were co-transfected with HA-UBC9 with Flag-SUMO2 encoding plasmids, and the lysates were immunoprecipitated with a GFP antibody. The KATNA1 K330R led to a significant reduction in the level of SUMOylation (Fig. 3*D*; the obvious SUMOylated bands indicated by arrow). Wildtype KATNA1 (GFP-KATNA1 WT) interacted with SUMO2 (Fig. 3*E*), but the significantly reduced signals from the sediments of K330R revealed that the KATNA1 K330R mutant disrupted the interaction between KATNA1 and SUMO2 (Fig. 3*F*). These data indicate that K330 is an essential residue for KATNA1 SUMOylation and SUMOylation of this residue

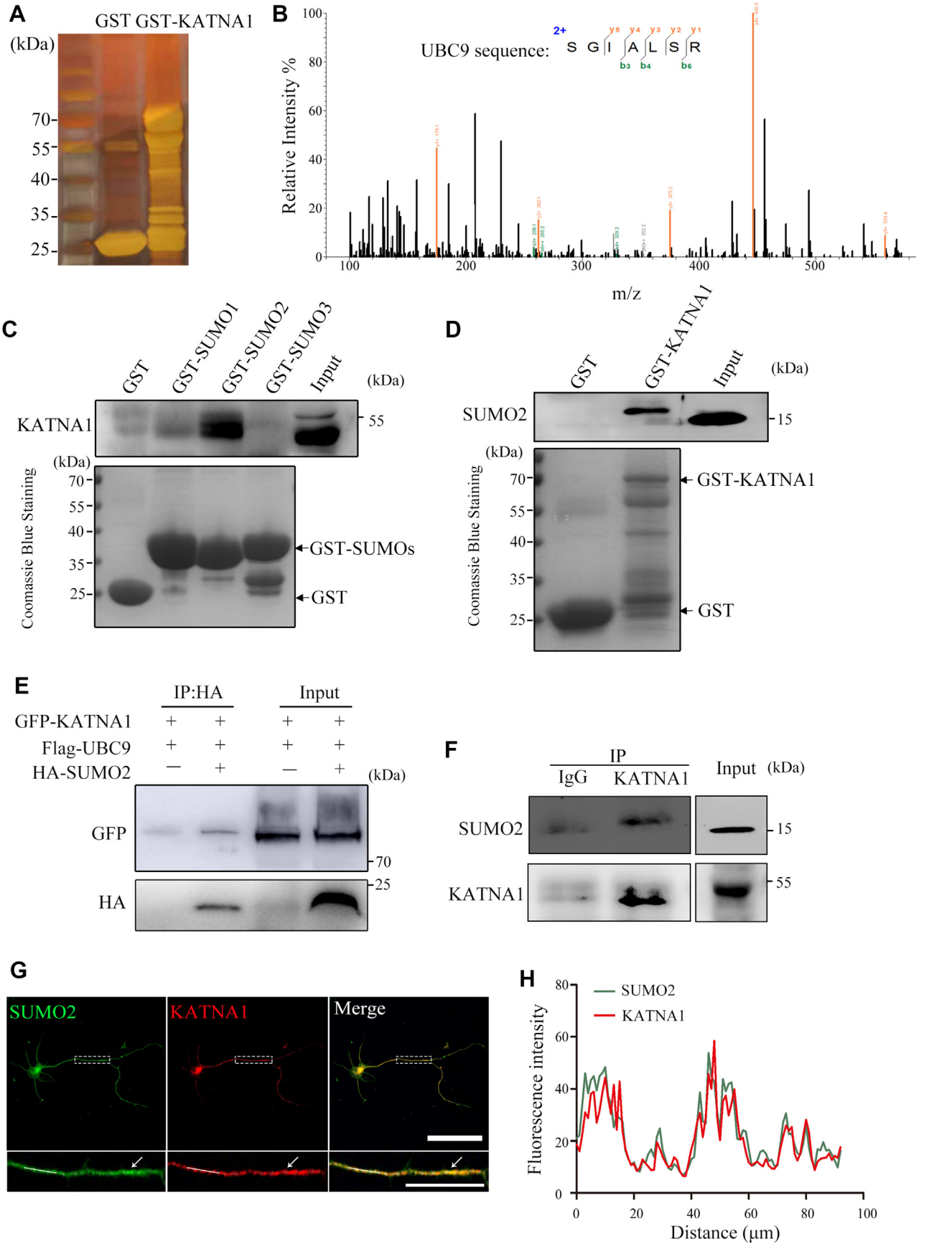

Figure 1. KATNA1 interacts with SUMO proteins. *A*, identification of KATNA1-binding proteins. Lysates from rat brain tissues were subjected to pulldown with GST or GST-KATNA1. Precipitated proteins were subjected to SDS-PAGE followed by staining with Fast Silver Stain Kit. , tandem mass spectrometry

has a direct effect on KATNA1-mediated microtubule severing activity.

SUMOylation promotes the microtubule severing activity of KATNA1

To further determine the role of K330 SUMOylation in KATNA1-mediated microtubule severing activity, we overexpressed mCherry-SUMO2 and Flag-UBC9 plasmids with different GFP-KATNA1 constructs in COS7 cells. Using immunofluorescence assays (Fig. 4*A*, circled cells indicating the transfected cells), we observed that overexpression of WT KATNA1 significantly induced microtubule severing relative to the control group or SUMO2 alone group, and co-transfection of KATNA1 with SUMO2 further increased the observed severing efficiency. However, KATNA1 K330R could not sever microtubules even when cotransfected with SUMO2 (Fig. 4*B*). These data further confirm that K330-mediated SUMOylation of KATNA1 promotes its microtubule severing activity.

Suppression of SUMOylation of KATNA1 abolishes the promoting effect in hippocampal neurite outgrowth

Next, we determined the role of KATNA1 SUMOylation in hippocampal neurite outgrowth. Because KATNA1 favors an acetylated microtubule cytoskeleton, we first examined the acetylation level of the hippocampal microtubules. As shown in Figure 5*A*, strong immunofluorescence signals were observed for acetylated microtubules in 2 to 4 DIV (days *in vitro*) neurons. To further understand the effect of KATNA1 SUMOylation on neurite outgrowth in hippocampal neurons, DIV2 primary hippocampal neuronal cells were sequentially transfected with GFP, GFP-KATNA1, and the mutants (Fig. 5*B*). The results showed that total length, axonal length, and dendritic length per neuron were significantly increased in KATNA1 WT and K77R and K157R overexpressing groups, but not in K330R and Pan mutant groups (Fig. 6, *A*–*C*). The number of tips (branches, Fig. 6, *D*–*F*) and neuronal complexity revealed by Sholl analysis (Fig. 6,*G*–*I*) showed the same trend as neurite length. These data demonstrate that KATNA1 promotes hippocampal neurite outgrowth, and the effect can be abolished if SUMOylation is absent or suppressed by mutation.

SUMOylation of KATNA1 enhances hippocampal neurite outgrowth

To further confirm the effect of KATNA1 SUMOylation on hippocampal neurite outgrowth, we overexpressed HA-UBC9 with or without WT or K330R GFP-KATNA1 or Flag-SUMO2. As shown in Figure 7, relative to the control or SUMO2 groups, overexpression of WT KATNA1 markedly promoted neurite outgrowth, with a concurrent increase in the neurite length (Fig. 8, *A*–*C*), the number of tips (Fig. 8, *D*–*F*), and neuronal complexity (Fig. 8, *G*–*I*). Moreover, co-overexpression of WT KATNA1 and SUMO2 further increased neurite outgrowth, whereas co-overexpression of K330R and SUMO2 exhibited no effects (Fig. 8). These data suggest that SUMOylation enhances the promoting effect of KATNA1 in regulating neurite outgrowth.

Discussion

In the current study, we show that KATNA1 is SUMOylated at K330. Disruption of this SUMOylation by mutation abolishes KATNA1 activity, whereas increased SUMOylation enhances the microtubule severing activity of KATNA1 and neurite outgrowth. The schematic diagram of this regulatory mechanism is shown in Figure 9. Our data supplement the landscape of KATNA1 regulation by posttranslational modification, which might play an important role in microtubule-related neuronal diseases.

SUMOylation is involved in the progression of numerous diseases, including cancer and Huntington's, Alzheimer's, and Parkinson's diseases (33, 34). Exportin-5 (XPO5) is modified by SUMO2, which increases the severity of hepatocellular carcinoma (35). In the cardiovascular system, SUMO2 activates calcium-regulated neurophosphatase NFAT signaling, which leads to myocardial inflammation and cardiac hypertrophy (36). SUMO2 is critical for cognitive processes, and knocking out the SUMO2 gene in mice leads to deficits in the memory process (37). A variety of proteins in the nervous system are SUMOylated (20). Here, we identify a novel regulatory mechanism wherein KATNA1 is SUMOylated at residue K330, and this SUMOylation is important for microtubule dynamics and neuronal outgrowth.

Cross talk between different posttranslational modifications is essential for fine-tuning protein activity (38). The tertiary structures and modification processes of SUMOylation are highly similar to those of ubiquitination (39). For example, the K293 residue in low-density lipoprotein receptor (IDOL) is modified by both SUMOylation and ubiquitination, wherein SUMOylation can counteract ubiquitination to increase the levels of IDOL (40). The deubiquitinating enzyme ubiquitin carboxy-terminal hydrolase 37 (USP37) is modified by SUMOylation and ubiquitination at different sites, and SUMOylation at K452 promotes subsequent ubiquitination of K148 and K389 (41). Katanin can be ubiquitinated. Antagonistic regulation of KATNA1 activity by E3 ubiquitin-protein ligase CHIP (CHIP) and the deubiquitinating enzyme ubiquitin carboxyl-terminal hydrolase 47 (USP47) influences

spectrum of a UBC9 peptide identified from pulldown sediments using GST-KATNA1 fusion protein. *C* and *D*, GST pulldown assays were performed with rat brain lysates. GST plasmids were constructed and proteins were purified (*lower panel*; the *arrow* points to the target protein). *E*, GFP-KATNA1 and HA-SUMO2 were overexpressed in 293T cells with Flag-UBC9. Coimmunoprecipitation with an anti-HA antibody was used to isolate proteins from the cell lysates, and the proteins were visualized using Western blotting and detected with anti-GFP and anti-HA antibodies. *F*, proteins were immunoprecipitated from rat brain lysates with a KATNA1 antibody, and the precipitates were immunostained with a SUMO2 antibody after Western blotting. *G*, immunocytochemistry for SUMO2 (*green*) and KATNA1 (*red*) was performed in hippocampal neurons at DIV3. White arrows indicate colocalization (*yellow* in merged image) in the neurite. The scale bar represents 20 μm. The *white rectangle* indicates the region chosen to show enlarged details (*lower panel*, the scale bar represents 10 μm). *H*, the fluorescence intensity profiles for KATNA1 and SUMO2 from the *white line* in the *lower panel* of (*G*).

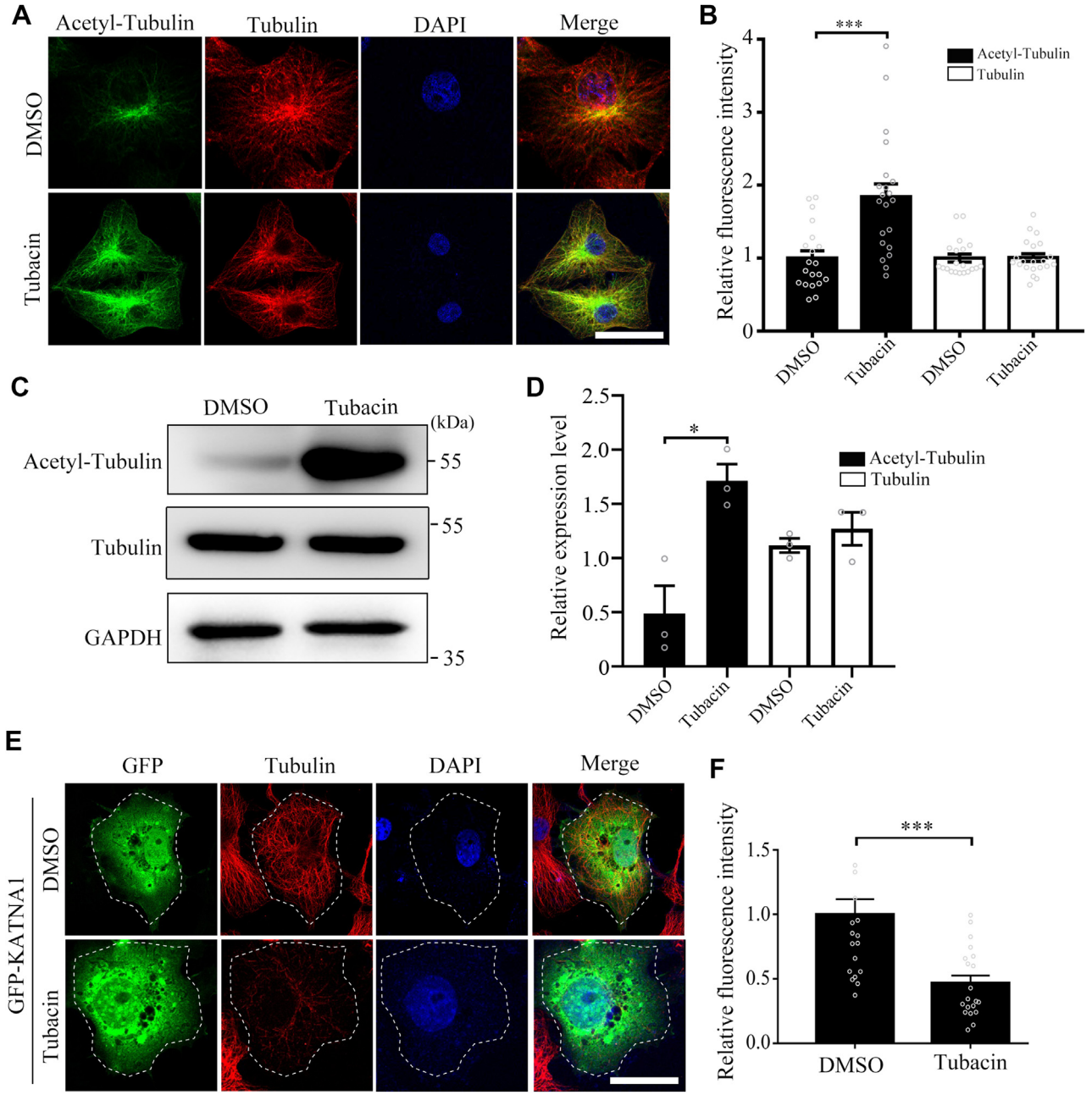

Figure 2. Acetylation of microtubules promotes severing by KATNA1. *A*, tubulin and acetylated tubulin (acetyl-tubulin) were detected using immunocytochemistry from COS7 cells treated with DMSO or Tubacin (10 nM). Representative images are shown. The scale bar represents 20 μm. *B*, the relative fluorescence intensity of tubulin and acetyl-tubulin was measured (n = 3, n corresponds to the number of independent experiments; cell number > 20/group for each replicate). Values represent mean±SD, tubulin was analyzed with nonparametric test, acetyl-tubulin was analyzed with one-way analysis of variance (ANOVA), ***$p < 0.001$. *C*, expression levels of acetyl-tubulin, tubulin, and GAPDH were detected using Western blotting for lysates from COS7 cells treated with DMSO or tubacin. *D*, relative protein expression of tubulin and acetyl-tubulin relative to GAPDH are shown. Values represent mean ± SD, the data were analyzed with nonparametric test, *$p < 0.05$. *E*, COS7 cells treated with DMSO or tubacin were transfected with GFP-KATNA1 (GFP fluorescence indicated the successful transfection, circled with *white line*) and were stained using immunofluorescent antibodies for tubulin (*red*) and GFP (*green*). Nuclei were stained with DAPI (*blue*). The scale bar represents 20 μm. *F*, the relative fluorescence intensities for tubulin in (*E*) were quantified (n = 3, n corresponds to the number of independent experiments; cell number > 20/group for each replicate). Values represent mean±SD; the data were analyzed with *t* test, ***$p < 0.001$. DMSO, dimethyl sulfoxide.

axonal growth in hippocampal neurons (26). In addition, the E3 ligase Cullin3 promotes degradation of Katanin to ensure mitotic spindle formation in nematodes (42). Here, we found that K330 is SUMOylated; K330 is not a reported ubiquitination site on KATNA1. Ubiquitination of KATNA1 regulates axonal growth in hippocampal neurons (26). In the present study, SUMOylation of KATNA1 promoted the development of neuronal protrusions. Whether or not K330 is ubiquitinated and the relationship between KATNA1 SUMOylation and ubiquitination need to be investigated further.

The stability and activity of Katanin are affected by phosphorylation (43). Phosphorylated Katanin exhibits decreased

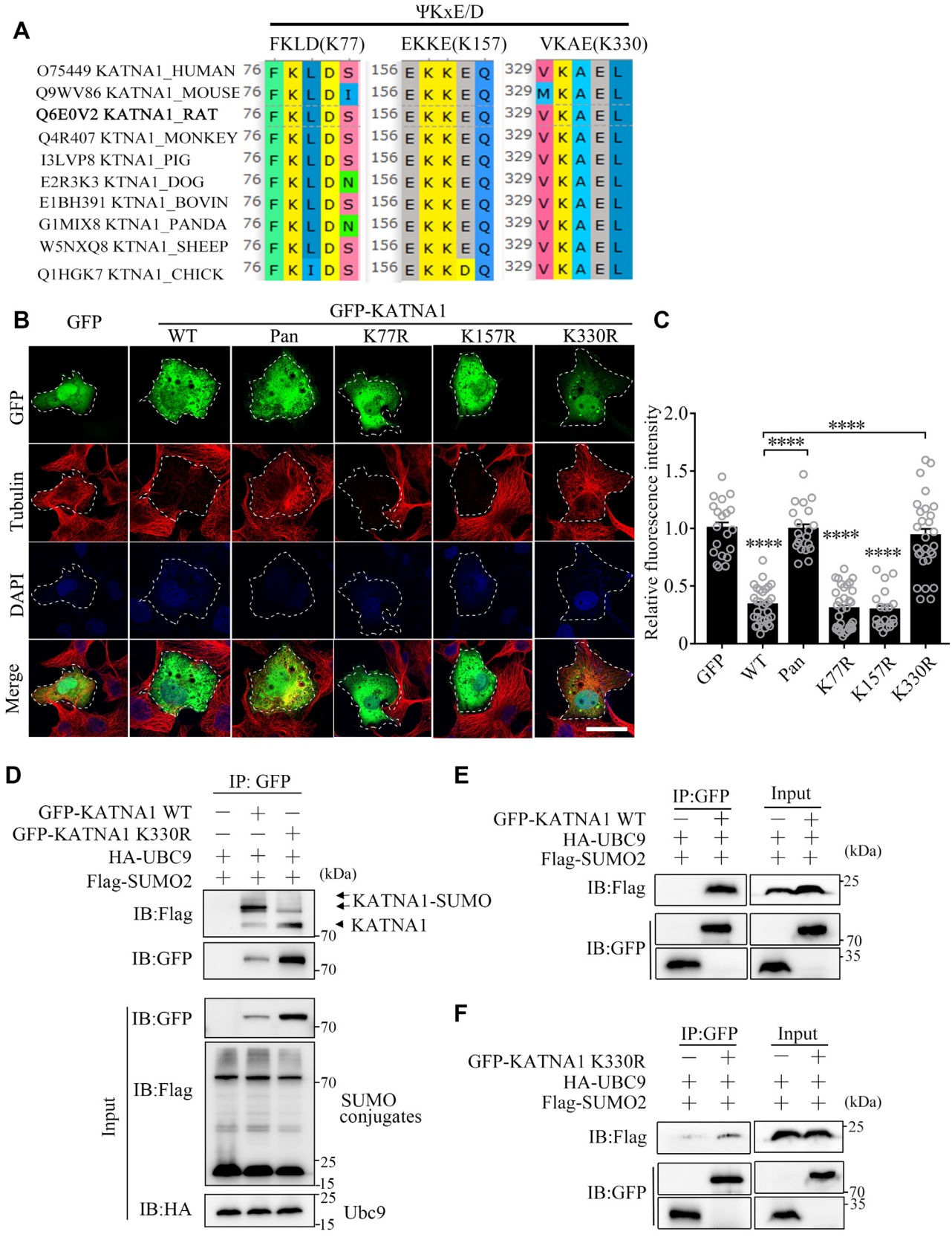

Figure 3. K330 is the SUMOylation site in KATNA1. *A*, protein sequence alignment analysis for KATNA1 shows three potential SUMOylation sites: FKLD (K77), EKKE (K157), and VKAE (K330). These sites are highly conserved in different vertebrate species. *B*, COS7 cells were transfected with GFP-KATNA1 or a mutant for 48 h (GFP fluorescence indicated the successfully transfected cells, circled with *white line*). The cells were stained using immunofluorescent antibodies for GFP (*green*) and tubulin (*red*). Nuclei were stained with DAPI (*blue*). The scale bar represents 20 μm. *C*, the relative fluorescence intensity of tubulin in COS7 cells was quantified (n = 3, n corresponds to the number of independent experiments; cell number > 20/group for each replicate). Values represent mean±SD; the data were analyzed with one-way analysis of variance (ANOVA), ****$p < 0.0001$. *D*, the SUMOylation level of K330R was reduced

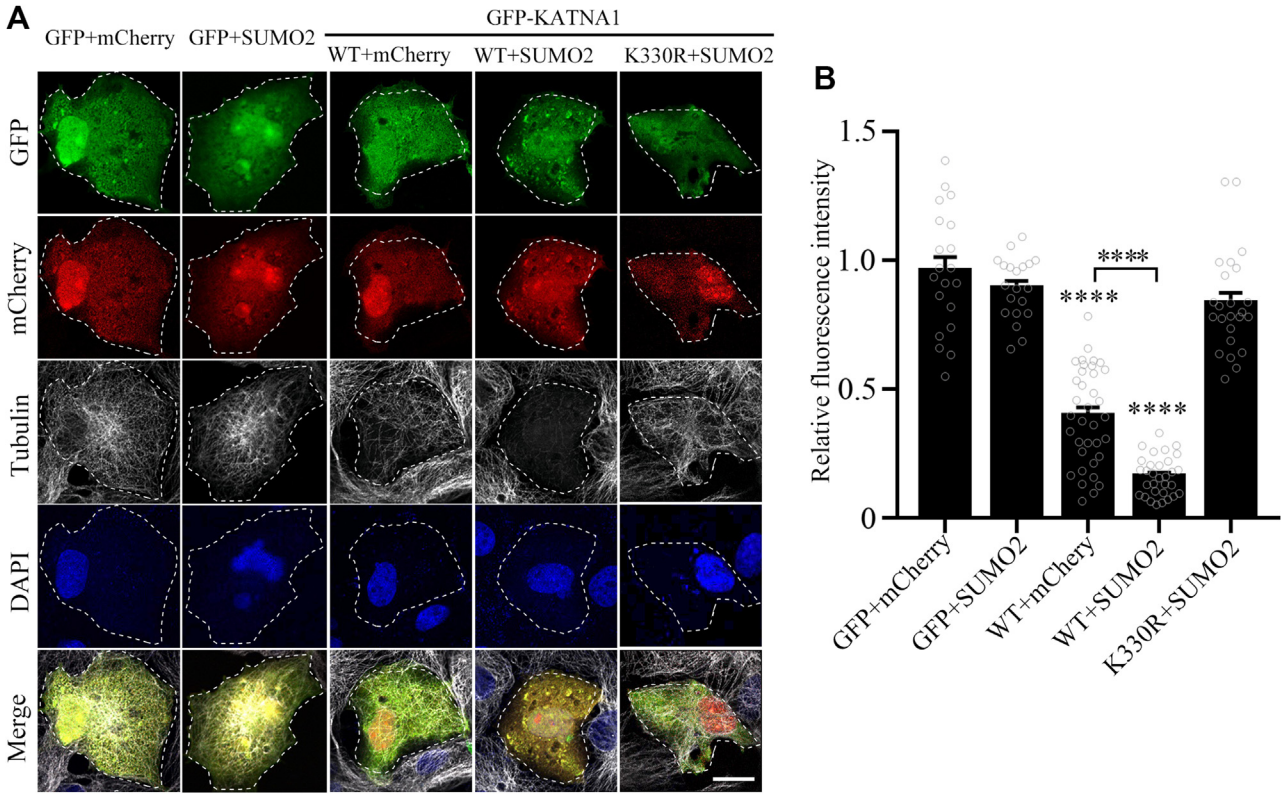

Figure 4. SUMOylation of KATNA1 promotes the microtubule severing activity of KATNA1. *A*, COS7 cells were transfected with different GFP-KATNA1 constructs with or without plasmids encoding mCherry-SUMO2; GFP or mCherry vector was used as control. Cells were stained with immunofluorescent antibodies for GFP (*green*), mCherry (*red*), and tubulin (*white*). GFP fluorescence indicated the successfully transfected cells, circled with *white line*. Nuclei were stained with DAPI (*blue*). The scale bar represents 20 μm. *B*, the relative fluorescence intensity of tubulin in COS7 cells was quantified. (n = 3; n corresponds to the number of independent experiments, cell number > 20/group for each replicate). Values represent mean ± SD; the data were analyzed with one-way analysis of variance (ANOVA), ****$p < 0.0001$.

microtubule severing ability, which affects mitotic spindle morphology in *Xenopus* (44). Phosphorylation of Katanin regulates the development of nematode embryos (27). Dual specificity tyrosine-phosphorylation-regulated kinase 2 (DYRK2) phosphorylates Katanin, which then promotes degradation of Katanin *via* the ubiquitination pathway (45). Phosphorylation is one of the most common posttranslational modifications, and phosphorylated proteins are involved in protein interactions, signal transduction, and protein degradation (46). Triangular regulation often exists between SUMOylation, ubiquitination, and phosphorylation, as is observed for Tau protein (47). We previously showed that collapsin response mediator protein 2, a microtubule assembly protein, is dephosphorylated at T514 and deSUMOylated at K374, which together promotes dendritic maturation (48). Hence, there is cross talk between phosphorylation and SUMOylation. How phosphorylation events affect KATNA1 SUMOylation (or the reverse) should be examined in future studies.

Protein interactions regulate KATNA1 activity; for example, abnormal spindle-like microcephaly-associated protein recruits KATNA1 and P80 to the negative end of microtubules, thereby limiting their growth during mitosis (49). RhoA-GTPase regulates KATNA1 expression to promote neurite outgrowth (50). Calcium ions inhibit the microtubule severing activity of p60, whereas its microtubule-binding activity is preserved in the presence of calcium (51). Cyclin-dependent kinase 5 phosphorylation of nuclear distribution protein nude-like 1 (NDEL1) promotes its interaction with KATNA1, which regulates the localization and activity of KATNA1 during neuronal migration (52). Calmodulin-regulated spectrin-associated proteins (CAMSAPs) are deposited at the negative end of microtubules to avoid spontaneous microtubule depolymerization, and Katanin binds to CAMSAPs to synergistically limit microtubule extension and maintain microtubule stability (53, 54). A-beta-S6 (ABS6) directly binds to and recruits Katanin to microtubules for severing (55), whereas Katanin-interacting protein (KIAA0556 or KATNIP) binds to Katanin and inhibits its activity (56). Therefore, interaction with proteins regulates the activity of Katanin through different pathways. Our findings that indicate that KATNA1 is SUMOylated and that

when compared with wildtype KATNA1 in 293T cells. Immunoprecipitation (IP) assay using 293T cells overexpressing HA-UBC9 and Flag-SUMO2 with GFP-KATNA1 or GFP-KATNA1 K330R. Protein lysates were coeluted with an anti-GFP antibody and detected with an anti-GFP antibody, anti-Flag antibody, and anti-HA antibody. (n = 3, n corresponds to the number of independent experiments). *E* and *F*, mutation from lysine to arginine at K330 disrupts the interaction between KATNA1 and SUMO2, co-IP experiment was same as in (*D*). (n = 3, n corresponds to the number of independent experiments).

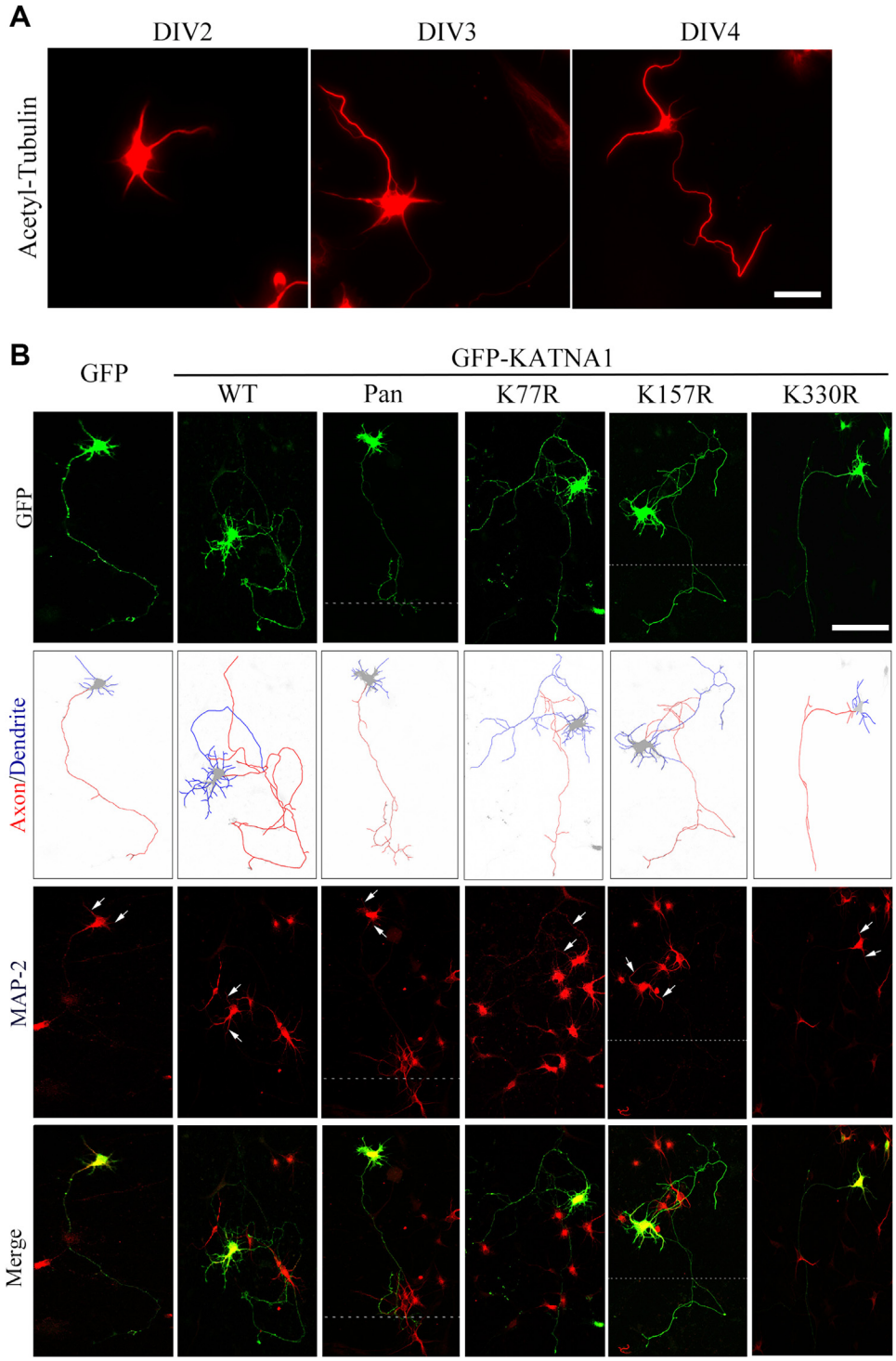

Figure 5. deSUMOylation of KATNA1 abolishes the promoting effect on hippocampal neurite outgrowth. *A*, DIV2–4 hippocampal neurons were immunostained to identify acetylated microtubules (*red*). The scale bar represents 100 μm. *B*, DIV2 hippocampal neurons were transfected with GFP, GFP-KATNA1, or a mutant for 48 h, and the neurons were immunostained with a GFP antibody (*green*) and MAP-2 (*red for dendrite*) to assess morphology. Dendrite was depicted with *blue line* and axon with *red line* for measurement. The *white dashed line* indicates the edge where two images were merged. Representative neurons are shown. The scale bar represents 100 μm.

SUMOylation enhances the microtubule cleaving activity of KATNA1 are supported in the literature. KATNA1 and Spastin are both in the AAA protease family and may regulate microtubule dynamics in a similar manner (57). Previously, we demonstrated that SUMOylation promotes maturation of neuronal dendritic spines and transport of α-amino-3-hydroxyl-5-methyl-4-isoxazolepropionic acid receptors. In addition, mutation of the Spastin SUMOylation site K427 abolishes its ability to cleave microtubules (14). The results from these studies indicate that mutation of SUMOylation

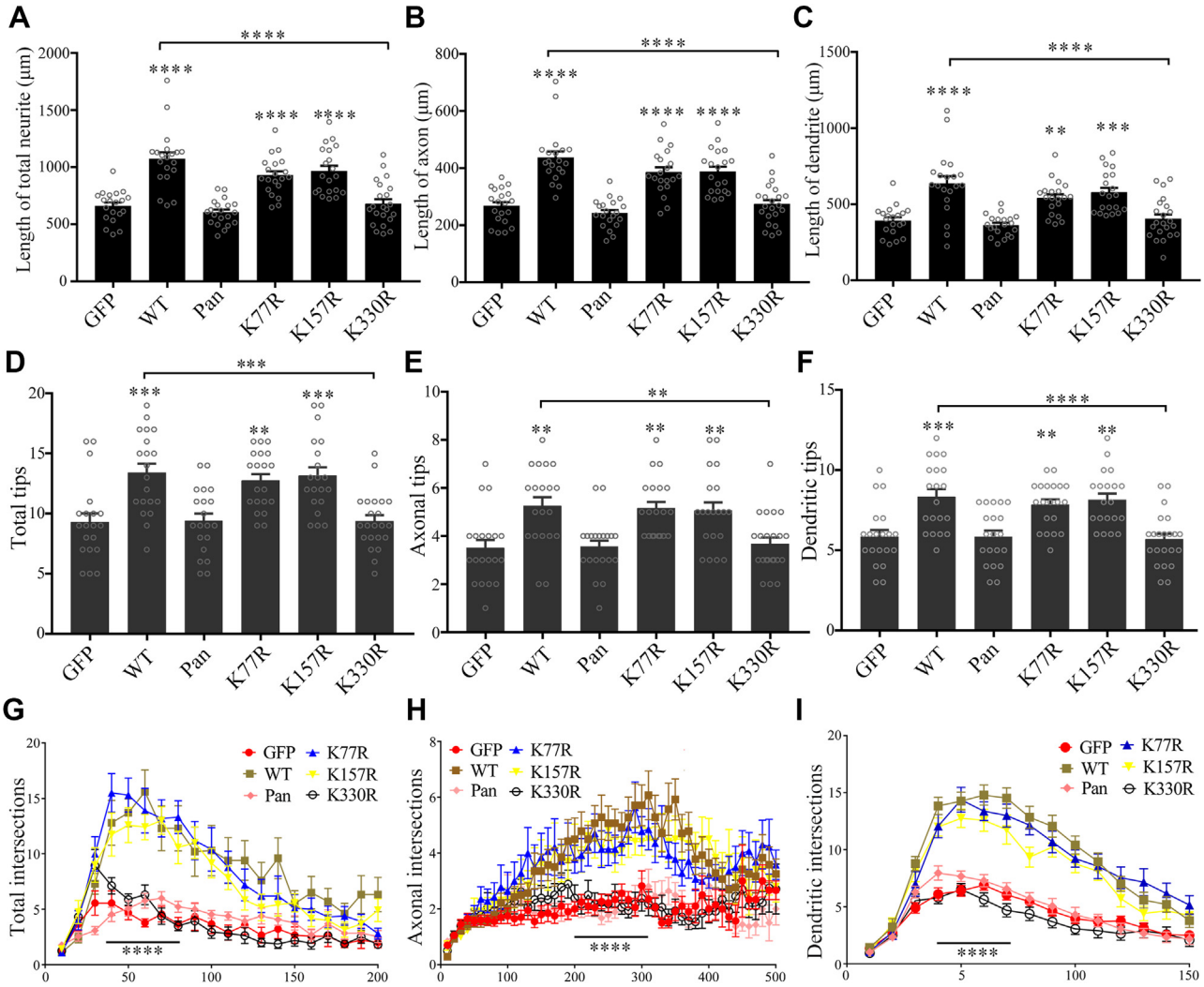

Figure 6. deSUMOylation of KATNA1 abolishes the promoting effect on hippocampal neurite outgrowth. Neurons treated in Figure 5 were subjected for measurement. The total length of neurite, axon, and dendrite *A–C*; tip numbers per neuron of total neurite, axon, and dendrite (*D–F*); and complexity (measured by Sholl analysis) (*G–I*) were calculated (n = 3, n corresponds to the number of independent experiments, neuron number > 30/group for each experimental replicate). Values represent mean±SD; the data were analyzed with one-way analysis of variance (ANOVA), $^{**}p < 0.01$, $^{***}p < 0.001$, $^{****}p < 0.0001$.

sites not only reduces the level of SUMOylation but also inhibits protein function.

Overall, we identified a novel mechanism regarding the SUMOylation of KATNA1 at K330 that promotes microtubule severing and neurite outgrowth, which provides new insight into the regulation of KATNA1 activity that may lead to novel therapeutic treatments for microcephaly and other neuronal developmental disorders.

Experimental procedures

Plasmid construction

Plasmids were constructed as described (58). The *KATNA1* (AY621629.1), *SUMO1* (NM_003352.8), *SUMO2* (NM_001005849.2), *SUMO3* (NM_006936.3), and *UBC9* (BC000427.2) genes were cloned from rat cDNA and validated *via* sequencing. *SUMO1* and *SUMO3* cDNA were inserted into a pGEX-5x-3 vector (MiaoLingBio, cat. no. #P0004), and *SUMO2* was subcloned into pGEX-5x-3, pLVX-mCherry-N1 (Takarabio, cat. no. #632562), pCMV-HA (Takarabio, cat. no. #635690), and pCMV-FLAG-C (MiaoLingBio, cat. no. #P1003). *KATNA1* was inserted into pEGFP-C1 (MiaoLingBio, cat. no. #P0134). *UBC9* was inserted into pCMV-FLAG-C and pCMV-HA. The corresponding mutant plasmids (K77R, K157R, K330R, and Pan) for GFP-KATNA1 were constructed using point mutation kits (Invitrogen, cat. no. #A14606). All constructs were verified after sequencing.

Protein purification and GST pulldown assays

Protein expression and GST pulldown assays were described (58). Briefly, GST-SUMO1, GST-SUMO2, and GST-SUMO3 were transformed into BL21 pLysS chemically competent cells (TransGen, cat. no. #CD701-02). Bacteria were cultured in 250 ml of Luria–Bertani medium (Sigma, cat. no. #L3152) containing ampicillin (Sigma, cat. no. #A5354) and were induced with 0.1 mM IPTG (Sigma, cat. no. #I6758) for 8 h at

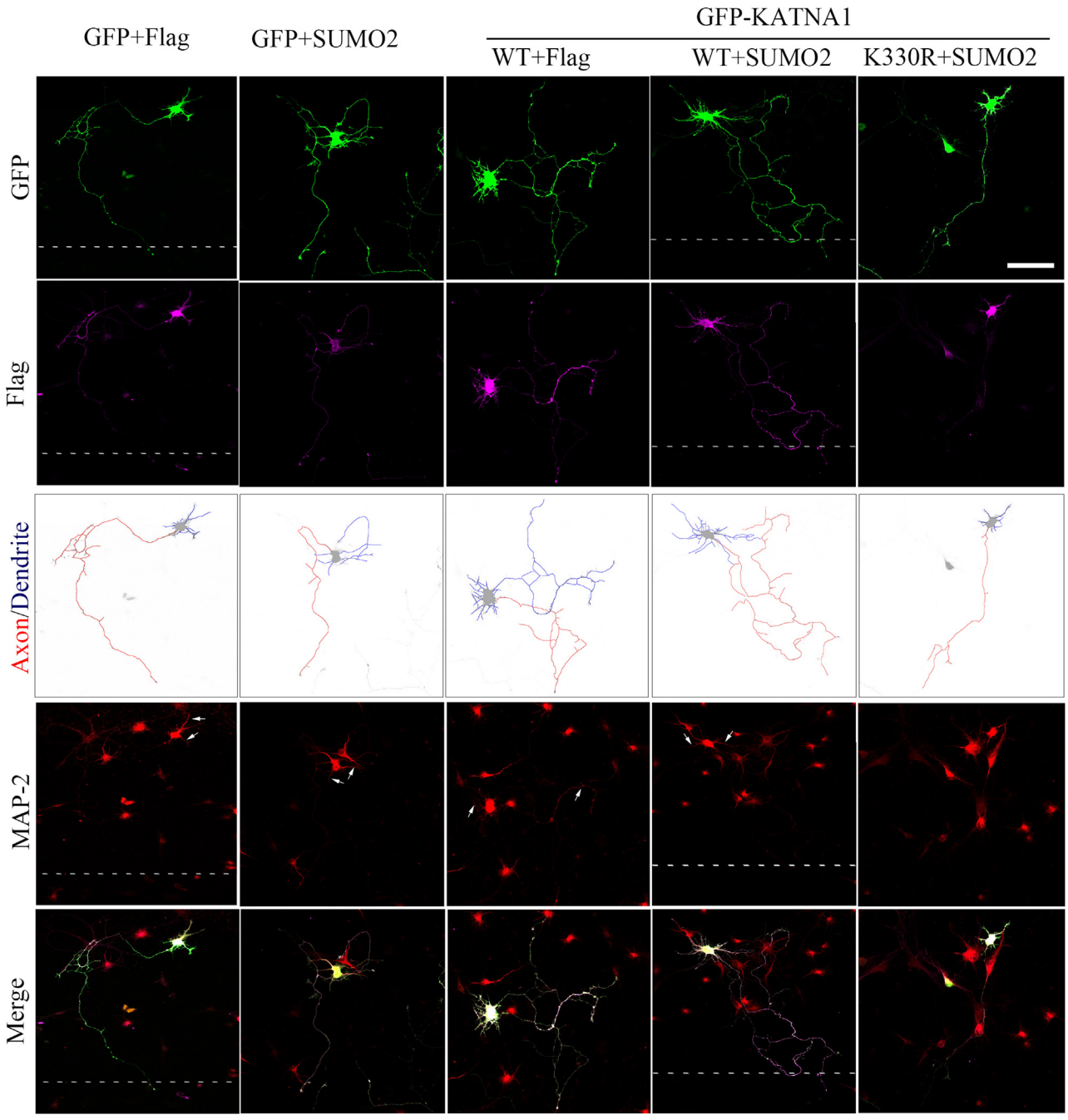

Figure 7. SUMOylation of KATNA1 enhances hippocampal neurite outgrowth. Hippocampal neurons were transfected with HA-UBC9 and GFP-KATNA1, or the K330R mutant (GFP vector as control), with or without Flag-SUMO2 (Flag vector as control) for 48 h. Neurons were stained with immunofluorescent antibodies for GFP (*green*), Flag (*purple*), and MAP-2 (*red for dendrite*). The *white dashed line* indicates the edge where two images were merged. The scale bar represents 100 μm.

30 °C. The bacteria were collected and 12.5 ml of lysis buffer (100 mM NaCl, 20 mM Tris-HCl, pH 7.0, and 5% glycerol), 1% Triton X-100, and a cocktail of protease inhibitors (Merck, cat. no. #HY-K100) consisting of 1 μM phenylmethylsulfonyl fluoride (Merck, cat. no. # PMSF-RO) were added. The bacteria were lysed on ice using sonication at 20% intensity for 1 h (every 15 min, the lysate was sonicated for 1 min, shaken for 30 s, and incubated on ice). After centrifugation of the lysate, 200 μl of glutathione agarose beads (Pierce Biotechnology, cat. no. #17-0756-01) were added to the supernatant. This mixture was inverted and mixed overnight at 4 °C, and the beads were retained after centrifugation. GST-fused protein (30–50 μg) was mixed with rat brain lysate, inverted overnight at 4 °C, and finally verified using Western blotting.

Cell culture and transfection

Primary hippocampal neurons were cultured as described (59). P0 (1-day-post-birth) Sprague Dawley rats were sacrificed by decapitation and then the hippocampus was taken from the

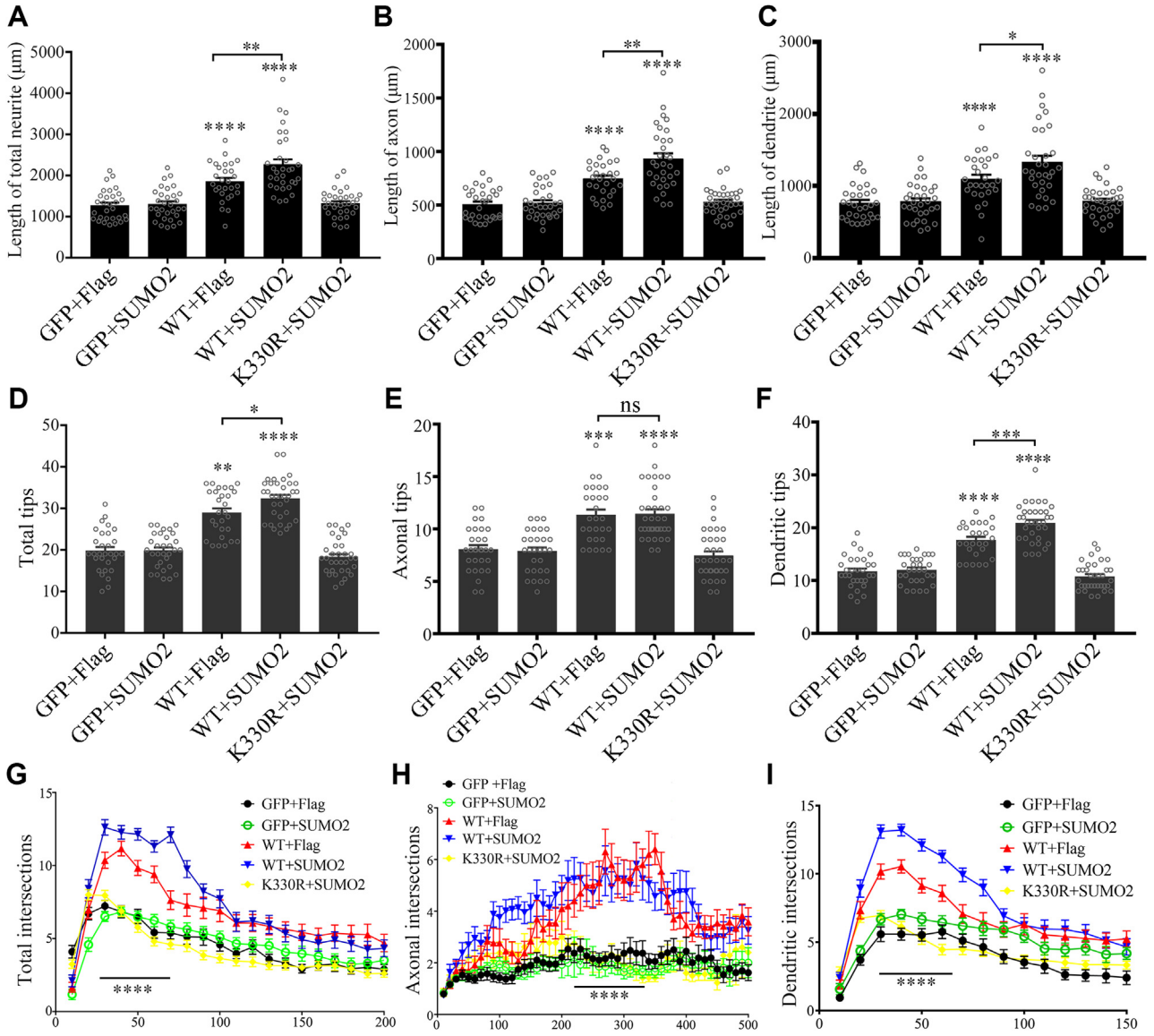

Figure 8. SUMOylation of KATNA1 enhances hippocampal neurite outgrowth. Neurons treated in Figure 7 were subjected for measurement. Total length of neurite, axon, and dendrite (*A–C*); tip numbers per neuron of total neurite, axon, and dendrite (*D–F*); and complexity (measured by Sholl analysis) (*G–I*) were calculated (n = 3, n corresponds to the number of independent experiments, neuron number > 30/group for each experimental replicate). Values represent mean ± SD; the data were analyzed with one-way analysis of variance (ANOVA), *$p < 0.05$, **$p < 0.01$, ***$p < 0.001$, ****$p < 0.0001$.

brains. A total of 80 rat pups were used in this study, 3 pups were used for each hippocampal culture. All rats were purchased from Southern Medical University (Production license: SCXK (Guangdong) 2016-0041, Use license: SYXK (Guangdong) 2016-016). All animal procedures were approved using the Guide for the Care and Use of Laboratory Animals from the NIH and were approved by the Jinan University Institutional Animal Care and Use Committee (Approval no. 20190310-05). The hippocampus was placed in 0.125% trypsin and was incubated in a 37 °C water bath for 20 min. Trypsin digestion was terminated with Dulbecco's modified Eagle medium (DMEM)/F12 (Gibco, cat. no. #11995065) with 10% fetal bovine serum (Gibco, cat. no. #10270-106). The cells were plated on glass coverslips coated with poly-D-lysine (Sigma, cat. no. #P6407) at a density of 1×10^4 cells/cm^2. After incubation for 30 min, 500 μl of DMEM/F12 with 10% fetal bovine serum was added to each well. The medium was replaced with neurobasal media supplemented with 2% B27 (Gibco, cat. no. #17504044) after 3 to 4 h. Cells were cultured at 37 °C with 5% CO_2. The plasmids were transfected at 2 DIV (days *in vitro*) using a calcium phosphate cell transfection kit (Beyotime, cat. no. #C0508) and were incubated for 48 h. The cells were fixed using 4% paraformaldehyde (Meilunbio, cat. no. #MA0192) for the immunofluorescence experiments.

COS7 and 293T cells were purchased from the National Collection of Authenticated Cell Cultures (STR certified), within five passages. The cells were cultured in DMEM medium (Gibco, cat. no. #C11995500BT) with 10% fetal bovine serum at 37 °C with 5% CO_2; the cells were transfected using lipofectamine 2000 (Invitrogen, cat. no. #11668019).

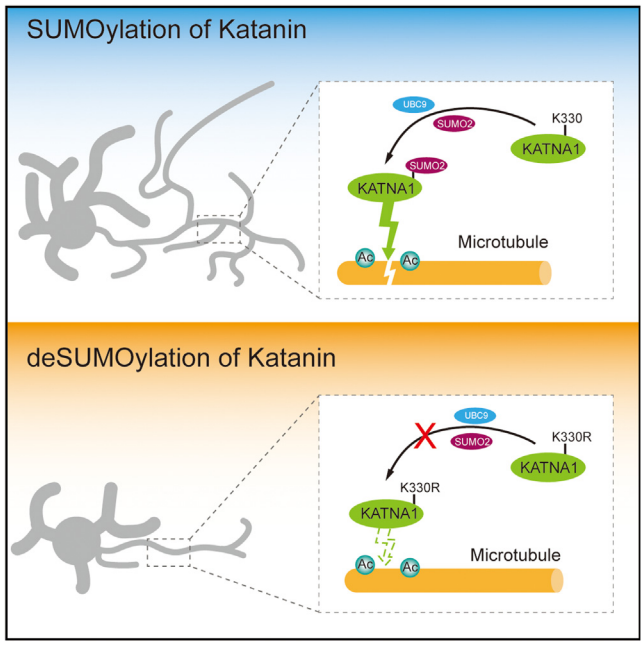

Figure 9. Schematic diagram of SUMOylation of KATNA1 regulated microtubule severing and neurite outgrowth. SUMOylation of KATNA1 at K330 can enhance the cleavage activity of KATNA1 and promote neurite outgrowth by cleaving acetylated (Ac) microtubules. Mutation of K330 to R alleviates the SUMOylation level of KATNA1, leading to reduced microtubule severing activity and neurite outgrowth.

Immunofluorescence

Immunofluorescence was described previously (60). Briefly, COS7 cells or hippocampal neurons were fixed using 4% paraformaldehyde for 40 min at 4 °C. The cells were then washed twice with TBS (Meilunbio, cat. no. #MA0141) with 0.1% Triton (TBST, Meilunbio, cat. no. #MB2486) at RT. The cells were blocked for 1 h at RT with 3% bovine serum albumin (Sigma, cat. no. #V900933-100G) in TBST. The cells were incubated with primary antibodies (GFP [Abcam, cat. no. #ab290, 1:1000], beta-Tubulin [Abcam, cat. no. #ab6046, 1:1000, for general tubulin staining], acetylated tubulin [Abcam, cat. no. #ab24610, 1:1000], KATNA1 [Proteintech, cat. no. #17560-1-AP, 1:200], MAP-2 [Abcam, cat. no. #ab5392, 1:500], Flag [Sigma, cat. no. #F9291, 1:3000], or SUMO2 [Novus, cat. no. #NBP2-44477, 1:1000]) at 4 °C overnight. Cells were washed three times and incubated with the corresponding secondary antibody (Thermo Fisher Scientific; Alexa Fluor 488, cat. no. #A-10680, RRID: AB 2534062; Alexa Fluor 555, cat. no. #A-21428, RRID: AB_2535849; Abcam, Alexa Fluor 647, cat. no. #ab150159) at RT for 1 h in the darkroom. The cells were fixed with NucBlue Fixed Cell ReadyProbes Reagent (DAPI, Electron Microscopy Science, cat. no. #17985-50) and imaged *via* confocal microscopy with an LSM 880 (Carl Zeiss).

Western blotting

Western blotting was performed as described (60). Briefly, 293T cells were lysed using lysis buffer (Beyotime, cat. no. #P0013). Equal amounts of total protein were loaded and run on a 10% SDS-PAGE gel and was transferred to a polyvinylidene fluoride membrane (Millipore, cat. no. #IPVH00010) for 1 h. The polyvinylidene fluoride membrane was blocked for 1 h at RT in TBS with 0.1% Tween-20 (TBST, Meilunbio, cat. no. #MB2483) and 5% skim milk (BD Difco, cat. no. #232100-500G). The membranes were incubated with primary antibodies (GFP [Abcam, cat. no. #ab290, 1:1000], HA [Sigma, cat. no. #H9658, 1:1000], KATNA1 [Proteintech, cat. no. #17560-1-AP, 1:500], beta-Tubulin [Abcam, cat. no. #ab6046, 1:5000], Flag [Sigma, cat. no. #F9291, 1:1000], GAPDH [Sigma, cat. no. #G9545, 1:5000], or acetylated tubulin [Abcam, cat. no. #ab179484, 1:5000]) at 4 °C overnight; the membranes were washed three times with TBST and incubated with the corresponding secondary antibody (1:5000, Abclonal Biotechnology, HRP Goat Anti-mouse IgG (H + L), cat. no. #AS003; HRP Goat Anti-rabbit IgG (H + L), cat. no. #AS014; HRP Goat Anti-rat IgG (H + L), cat. no. #AS028) at RT for 1 h. Membranes were exposed to BeyoECL Plus (Beyotime, cat. no. #P0018S) for visualization.

Neuronal morphometry analysis

Neuronal morphometry was performed as reported (60). Briefly, GFP-overexpressed hippocampal neurons were immunostained with antibodies against GFP for total neurite and MAP2 for dendrites, then neurons were imaged in a blinded manner with Axio Observer Z1 (Carl Zeiss). The parameters of total neurite length per neuron, axonal/dendritic length per neuron, total tips per neuron, axonal/dendritic tips per neuron from at least 20 neurons per group were calculated by Image Pro Plus 6 software (Media Cybernetics).

Sholl analysis

Sholl analysis was carried out as reported (61, 62). Briefly, the images were randomly collected using an LSM 880 confocal microscope (Carl Zeiss), and each group contained at least 20 neurons. ImageJ (NIH) was used to change the image to 8-bit grayscale, and the modified images were saved. The saved image was opened in NeuronJ (63), the neuron trajectory was drawn. Taking the neuron cell body as the center, a circle was drawn with a radius that contained all the protrusions, and this image was used for subsequent calculations. Data were exported to GraphPad Prism 5 for measurement. The groups were blinded for measurement and then unblinded for group labels.

Mass spectrometry

Mass spectrometry was used to analyze sediments from GST-KATNA1 pulldown assays. The gel was digested with trypsin. GST and GST-KATNA1 samples were used for nano-liquid chromatography–tandem mass spectrometry (LC-MS/MS) analysis. After chromatographic separation, the samples were analyzed using a Q Exactive mass spectrometer (Thermo Fisher Scientific) for 60 min. The detection method was positive ion mode, the precursor ion scan range was 300 to 1800 *m/z*, the resolution of the primary mass spectrum was 70,000 at 200 *m/z*, the automatic gain control target was 1e6,

the Maximum IT was 50 ms, and the dynamic exclusion time (Dynamic exclusion) was 60 s. MS/MS spectra were searched against the UniProtKB database using the MASCOT engine (Matrix Science; version 2.4).

Statistical analysis

All data are presented as the means ± SD from at least three independent experiments. GraphPad Prism 7 was used to generate graphs and statistics; ImageJ (NIH) was used to measure the microtubule fluorescence intensity in COS7 cells. All data in this study used D'Agostino and Pearson normality test for normality test. For data that conform to the normal distribution, analyses were performed using a *t* test or one-way analysis of variance (ANOVA). For data that do not conform to a normal distribution, a nonparametric test (Wilcoxon rank sum test) was applied. All tests are two-tailed tests. $p < 0.05$ indicates statistical significance, ($^{*}p < 0.05$, $^{**}p < 0.01$, $^{***}p < 0.001$, $^{****}p < 0.0001$).

Data availability

The data that support the findings of this study are available from the corresponding author upon reasonable request.

Acknowledgments—This work was supported by the National Natural Science Foundation of China (nos. 32071033, 81771331, and 32170977).

Author contributions—G. Z., M. T. conceptualization; Y. L. methodology; J. Z. software; Z. C., H. Y., J. Y., Y. Z. validation; S. L., Y. L., Z. C. data curation; S. L. writing – original draft; H. Y., J. Y., Y. Z., H. L., G. Z., M. T. writing – review & editing; J. Z. visualization; M. T. supervision; M. T. project administration.

Conflict of interest—The authors declare that they have no conflicts of interest with the contents of this article.

Abbreviations—The abbreviations used are: DIV, days *in vitro*; DMEM, Dulbecco's modified Eagle medium; IP, immunoprecipitation; KATNA1, Katanin p60 ATPase-containing subunit A1; SUMO, small ubiquitin-like modifier.

References

1. Kuo, Y. W., and Howard, J. (2021) Cutting, amplifying, and aligning microtubules with severing enzymes. *Trends Cell Biol.* **31**, 50–61
2. Zehr, E. A., Szyk, A., Szczesna, E., and Roll-Mecak, A. (2020) Katanin grips the β-tubulin tail through an electropositive double spiral to sever microtubules. *Dev. Cell* **52**, 118–131.e116
3. Hu, W. F., Pomp, O., Ben-Omran, T., Kodani, A., Henke, K., Mochida, G. H., *et al.* (2014) Katanin p80 regulates human cortical development by limiting centriole and cilia number. *Neuron* **84**, 1240–1257
4. McNally, F. J., and Roll-Mecak, A. (2018) Microtubule-severing enzymes: from cellular functions to molecular mechanism. *J. Cell Biol.* **217**, 4057–4069
5. Sudo, H., and Baas, P. W. (2010) Acetylation of microtubules influences their sensitivity to severing by katanin in neurons and fibroblasts. *J. Neurosci.* **30**, 7215–7226
6. Sudo, H., and Baas, P. W. (2011) Strategies for diminishing katanin-based loss of microtubules in tauopathic neurodegenerative diseases. *Hum. Mol. Genet.* **20**, 763–778
7. Ikegami, K., and Setou, M. (2010) Unique post-translational modifications in specialized microtubule architecture. *Cell Struct. Funct.* **35**, 15–22
8. Geoffroy, C. G., and Zheng, B. (2014) Myelin-associated inhibitors in axonal growth after CNS injury. *Curr. Opin. Neurobiol.* **27**, 31–38
9. Li, H. J., Sun, Z. L., Yang, X. T., Zhu, L., and Feng, D. F. (2017) Exploring optic nerve axon regeneration. *Curr. Neuropharmacol.* **15**, 861–873
10. Riano, E., Martignoni, M., Mancuso, G., Cartelli, D., Crippa, F., Toldo, I., *et al.* (2009) Pleiotropic effects of spastin on neurite growth depending on expression levels. *J. Neurochem.* **108**, 1277–1288
11. Ghosh, D. K., Dasgupta, D., and Guha, A. (2012) Models, regulations, and functions of microtubule severing by katanin. *ISRN Mol. Biol.* **2012**, 596289
12. Lombino, F. L., Muhia, M., Lopez-Rojas, J., Brill, M. S., Thies, E., Ruschkies, L., *et al.* (2019) The microtubule severing protein katanin regulates proliferation of neuronal progenitors in embryonic and adult neurogenesis. *Sci. Rep.* **9**, 15940
13. Shin, S. C., Im, S. K., Jang, E. H., Jin, K. S., Hur, E. M., and Kim, E. E. (2019) Structural and molecular basis for katanin-mediated severing of glutamylated microtubules. *Cell Rep.* **26**, 1357–1367.e1355
14. Ji, Z. S., Liu, Q. L., Zhang, J. F., Yang, Y. H., Li, J., Zhang, G. W., *et al.* (2020) SUMOylation of spastin promotes the internalization of GluA1 and regulates dendritic spine morphology by targeting microtubule dynamics. *Neurobiol. Dis.* **146**, 105133
15. Chen, K., Ye, Y., Ji, Z., Tan, M., Li, S., Zhang, J., *et al.* (2014) Katanin p60 promotes neurite growth and collateral formation in the hippocampus. *Int. J. Clin. Exp. Med.* **7**, 2463–2470
16. Matunis, M. J., and Rodriguez, M. S. (2016) Concepts and methodologies to study protein SUMOylation: an overview. *Met. Mol. Biol.* **1475**, 3–22
17. Nayak, A., and Müller, S. (2014) SUMO-Specific proteases/isopeptidases: SENPs and beyond. *Genome Biol.* **15**, 422
18. Gujjula, R., Veeraiah, S., Kumar, K., Thakur, S. S., Mishra, K., and Kaur, R. (2016) Identification of components of the SUMOylation machinery in Candida glabrata: role of the desumoylation peptidase CgUlp2 in virulence. *J. Biol. Chem.* **291**, 19573–19589
19. Hannoun, Z., Greenhough, S., Jaffray, E., Hay, R. T., and Hay, D. C. (2010) Post-translational modification by SUMO. *Toxicology* **278**, 288–293
20. Wilkinson, K. A., Nakamura, Y., and Henley, J. M. (2010) Targets and consequences of protein SUMOylation in neurons. *Brain Res. Rev.* **64**, 195–212
21. Yau, T. Y., Molina, O., and Courey, A. J. (2020) SUMOylation in development and neurodegeneration. *Development* **147**, dev175703
22. Ryu, J., Cho, S., Park, B. C., and Lee, D. H. (2010) Oxidative stress-enhanced SUMOylation and aggregation of ataxin-1: implication of JNK pathway. *Biochem. Biophys. Res. Commun.* **393**, 280–285
23. Bernstock, J. D., Ye, D. G., Griffin, A., Lee, Y. J., Lynch, J., Latour, L. L., *et al.* (2017) Cerebral ischemia increases small ubiquitin-like modifier conjugation within human penumbral tissue: radiological-pathological correlation. *Front. Neurol.* **8**, 738
24. Schorova, L., and Martin, S. (2016) Sumoylation in synaptic function and dysfunction. *Front. synaptic Neurosci.* **8**, 9
25. Khan, F. A., Pandupuspitasari, N. S., Huang, C. J., Hao, X., and Zhang, S. (2016) SUMOylation: a link to future therapeutics. *Curr. Issues Mol. Biol.* **18**, 49–56
26. Yang, S. W., Oh, K. H., Park, E., Chang, H. M., Park, J. M., Seong, M. W., *et al.* (2013) USP47 and C terminus of Hsp70-interacting protein (CHIP) antagonistically regulate katanin-p60-mediated axonal growth. *J. Neurosci.* **33**, 12728–12738
27. Joly, N., Beaumale, E., Van Hove, L., Martino, L., and Pintard, L. (2020) Phosphorylation of the microtubule-severing AAA+ enzyme Katanin regulates C. elegans embryo development. *J. Cell Biol.* **219**, e201912037
28. Zhao, Q., Xie, Y., Zheng, Y., Jiang, S., Liu, W., Mu, W., *et al.* (2014) GPS-SUMO: a tool for the prediction of sumoylation sites and SUMO-interaction motifs. *Nucl. Acids Res.* **42**, W325–W330
29. Xue, Y., Zhou, F., Fu, C., Xu, Y., and Yao, X. (2006) SUMOsp: a web server for sumoylation site prediction. *Nucl. Acids Res.* **34**, W254–W257
30. Zhao, N., Sebastiano, V., Moshkina, N., Mena, N., Hultquist, J., Jimenez-Morales, D., *et al.* (2018) Influenza virus infection causes global RNAPII termination defects. *Nat. Struct. Mol. Biol.* **25**, 885–893

31. Way, G., Xiong, Z., Wang, G., Dai, H., Zheng, S., Garcia-Sastre, A., *et al.* (2020) A novel SUMOylation site in the influenza a virus NS1 protein identified with a highly sensitive FRET assay. *J. Biotechnol.* **323**, 121–127
32. Geiss-Friedlander, R., and Melchior, F. (2007) Concepts in sumoylation: a decade on. *Nat. Rev. Mol. Cell Biol.* **8**, 947–956
33. Chen, X., Zhang, Y., Wang, Q., Qin, Y., Yang, X., Xing, Z., *et al.* (2021) The function of SUMOylation and its crucial roles in the development of neurological diseases. *FASEB J.* **35**, e21510
34. Tokarz, P., and Woźniak, K. (2021) SENP proteases as potential targets for cancer therapy. *Cancer* **13**, 2059
35. Lin, D., Fu, Z., Yang, G., Gao, D., Wang, T., Liu, Z., *et al.* (2020) Exportin-5 SUMOylation promotes hepatocellular carcinoma progression. *Exp. Cell Res.* **395**, 112219
36. Rangrez, A. Y., Borlepawar, A., Schmiedel, N., Deshpande, A., Remes, A., Kumari, M., *et al.* (2020) The E3 ubiquitin ligase HectD3 attenuates cardiac hypertrophy and inflammation in mice. *Commun. Biol.* **3**, 562
37. Yu, S., Galeffi, F., Rodriguiz, R. M., Wang, Z., Shen, Y., Lyu, J., *et al.* (2020) Small ubiquitin-like modifier 2 (SUMO2) is critical for memory processes in mice. *FASEB J.* **34**, 14750–14767
38. Zhang, Y., and Zeng, L. (2020) Crosstalk between ubiquitination and other post-translational protein modifications in plant Immunity. *Plant Commun.* **1**, 100041
39. Liebelt, F., and Vertegaal, A. C. (2016) Ubiquitin-dependent and independent roles of SUMO in proteostasis. *Am. J. Physiol. Cell Physiol.* **311**, C284–C296
40. Wang, J. Q., Lin, Z. C., Li, L. L., Zhang, S. F., Li, W. H., Liu, W., *et al.* (2020) SUMOylation of the ubiquitin ligase IDOL decreases LDL receptor levels and is reversed by SENP1. *J. Biol. Chem.* **296**, 100032
41. Lamoliatte, F., McManus, F. P., Maarifi, G., Chelbi-Alix, M. K., and Thibault, P. (2017) Uncovering the SUMOylation and ubiquitylation crosstalk in human cells using sequential peptide immunopurification. *Nat. Commun.* **8**, 14109
42. Beard, S. M., Smit, R. B., Chan, B. G., and Mains, P. E. (2016) Regulation of the MEI-1/MEI-2 microtubule-severing katanin complex in early Caenorhabditis elegans development. *G3 (Bethesda, Md.* **6**, 3257–3268
43. Whitehead, E., Heald, R., and Wilbur, J. D. (2013) N-terminal phosphorylation of p60 katanin directly regulates microtubule severing. *J. Mol. Biol.* **425**, 214–221
44. Loughlin, R., Wilbur, J. D., McNally, F. J., Nédélec, F. J., and Heald, R. (2011) Katanin contributes to interspecies spindle length scaling in Xenopus. *Cell* **147**, 1397–1407
45. Maddika, S., and Chen, J. (2009) Protein kinase DYRK2 is a scaffold that facilitates assembly of an E3 ligase. *Nat. Cell Biol.* **11**, 409–419
46. Ardito, F., Giuliani, M., Perrone, D., Troiano, G., and Lo Muzio, L. (2017) The crucial role of protein phosphorylation in cell signaling and its use as targeted therapy (Review). *Int. J. Mol. Med.* **40**, 271–280
47. Luo, H. B., Xia, Y. Y., Shu, X. J., Liu, Z. C., Feng, Y., Liu, X. H., *et al.* (2014) SUMOylation at K340 inhibits tau degradation through deregulating its phosphorylation and ubiquitination. *Proc. Natl. Acad. Sci. U. S. A.* **111**, 16586–16591
48. Yu, J., Moutal, A., Dorame, A., Bellampalli, S. S., Chefdeville, A., Kanazawa, I., *et al.* (2019) Phosphorylated CRMP2 regulates spinal nociceptive neurotransmission. *Mol. Neurobiol.* **56**, 5241–5255
49. Jiang, K., Rezabkova, L., Hua, S., Liu, Q., Capitani, G., Altelaar, A. F. M., *et al.* (2017) Microtubule minus-end regulation at spindle poles by an ASPM-katanin complex. *Nat. Cell Biol.* **19**, 480–492
50. Tan, D., Zhang, H., Deng, J., Liu, J., Wen, J., Li, L., *et al.* (2020) RhoA-GTPase modulates neurite outgrowth by regulating the expression of spastin and p60-katanin. *Cells* **9**, 230
51. Iwaya, N., Akiyama, K., Goda, N., Tenno, T., Fujiwara, Y., Hamada, D., *et al.* (2012) Effect of Ca2+ on the microtubule-severing enzyme p60-katanin. Insight into the substrate-dependent activation mechanism. *FEBS J.* **279**, 1339–1352
52. Toyo-Oka, K., Sasaki, S., Yano, Y., Mori, D., Kobayashi, T., Toyoshima, Y. Y., *et al.* (2005) Recruitment of katanin p60 by phosphorylated NDEL1, an LIS1 interacting protein, is essential for mitotic cell division and neuronal migration. *Hum. Mol. Genet.* **14**, 3113–3128
53. Jiang, K., Faltova, L., Hua, S., Capitani, G., Prota, A. E., Landgraf, C., *et al.* (2018) Structural Basis of Formation of the Microtubule Minus-End-Regulating CAMSAP-Katanin Complex. *Structure* **26**, 375–382. e374
54. Jiang, K., Hua, S., Mohan, R., Grigoriev, I., Yau, K. W., Liu, Q., *et al.* (2014) Microtubule minus-end stabilization by polymerization-driven CAMSAP deposition. *Dev. Cell* **28**, 295–309
55. Li, Y., Deng, M., Liu, H., Li, Y., Chen, Y., Jia, M., *et al.* (2020) ABNORMAL SHOOT 6 interacts with KATANIN 1 and SHADE AVOIDANCE 4 to promote cortical microtubule severing and ordering in arabidopsis. *J. Integr. Plant Biol.* **63**, 646–661
56. Andrés-Benito, P., Delgado-Morales, R., and Ferrer, I. (2018) Altered regulation of KIAA0566, and katanin signaling expression in the locus coeruleus with neurofibrillary tangle pathology. *Front. Cell. Neurosci.* **12**, 131
57. Kuo, Y. W., Trottier, O., Mahamdeh, M., and Howard, J. (2019) Spastin is a dual-function enzyme that severs microtubules and promotes their regrowth to increase the number and mass of microtubules. *Proc. Natl. Acad. Sci. U. S. A.* **116**, 5533–5541
58. Ji, Z., Zhang, G., Chen, L., Li, J., Yang, Y., Cha, C., *et al.* (2018) Spastin interacts with CRMP5 to promote neurite outgrowth by controlling the microtubule dynamics. *Dev. Neurobiol.* **78**, 1191–1205
59. Jiang, T., Zhang, G., Liang, Y., Cai, Z., Liang, Z., Lin, H., *et al.* (2020) PlexinA3 interacts with CRMP2 to mediate Sema3A signalling during dendritic growth in cultured cerebellar granule neurons. *Neuroscience* **434**, 83–92
60. Jiang, T., Cai, Z., Ji, Z., Zou, J., Liang, Z., Zhang, G., *et al.* (2020) The lncRNA MALAT1/miR-30/spastin axis regulates hippocampal neurite outgrowth. *Front. Cell Neurosci.* **14**, 555747
61. Binley, K. E., Ng, W. S., Tribble, J. R., Song, B., and Morgan, J. E. (2014) Sholl analysis: a quantitative comparison of semi-automated methods. *J. Neurosci. Met.* **225**, 65–70
62. Yang, Y., Wang, Z. H., Jin, S., Gao, D., Liu, N., Chen, S. P., *et al.* (2016) Opposite monosynaptic scaling of BLP-vCA1 inputs governs hopefulness- and helplessness-modulated spatial learning and memory. *Nat. Commun.* **7**, 11935
63. Meijering, E., Jacob, M., Sarria, J. C., Steiner, P., Hirling, H., and Unser, M. (2004) Design and validation of a tool for neurite tracing and analysis in fluorescence microscopy images. *Cytometry A* **58**, 167–176